

Collective oscillations in a single-wall carbon nanotube excited by fast electronsThomas Stöckli,^{*,†} Jean-Marc Bonard, and André Châtelain*Institut de Physique Expérimentale, Département de Physique, Ecole Polytechnique Fédérale de Lausanne, CH-1015 Lausanne, Switzerland*

Zhong Lin Wang

School of Materials Science and Engineering, Georgia Institute of Technology, Atlanta, Georgia 30332-0245

Pierre Stadelmann

Centre Interdépartemental de Microscopie Electronique, Ecole Polytechnique Fédérale de Lausanne, CH-1015 Lausanne, Switzerland

(Received 29 August 2000; published 31 August 2001)

Electron energy loss spectroscopy is a well adapted tool for the investigation of the valence excitations of individual nanometer-size particles. The interpretation of the loss spectra of such small particles, however, relies in most cases on a quantitative comparison with simulated excitation probabilities. Here we present a formalism developed for the interpretation of the energy loss data of single-wall carbon nanotubes based on the hydrodynamic theory of plasmon excitations by high-energy electrons. The nanotubes are modeled as a two-dimensional electron gas confined on the circumference of a cylinder. The plasmon excitation probabilities, directly comparable to measurements, are discussed for various parameters.

DOI: 10.1103/PhysRevB.64.115424

PACS number(s): 73.20.Mf, 34.50.Bw, 73.61.Wp

I. INTRODUCTION

One of the most fascinating aspects about single-wall carbon nanotubes¹ is that their electronic properties critically depend on their geometry. Experimentally, such theoretical predictions²⁻⁴ have proven difficult to validate since even the most recent production methods⁵⁻⁸ yield a mixture of tubes of different helicities and diameters. Purification methods⁹⁻¹⁴ have been proposed but a separation of the tubes according to helicity and radius is not yet possible. One way to overcome these experimental problems consists in the investigation of the properties of individual particles. This requires local probe techniques capable of imaging a nanotube with atomic resolution and of measuring at the same time its physical properties. Scanning tunneling microscopy (STM), for instance, fulfills these conditions and has proven useful in the study of carbon nanotubes. Important information about the electronic structure and its dependence on the geometry of the nanotube has thus been obtained.¹⁵⁻²⁰ Another local probe technique, atomic force microscopy (AFM) has also proven useful in the study of carbon nanotubes. The ability of this technique to apply a force on nanometer-size particles has been used to determine the mechanical properties of various types of carbon nanotubes.^{21,22}

Despite these recent advances in the characterization of carbon nanotubes, there is still a need for additional information. An alternative local probe technique such as electron energy loss spectroscopy (EELS) in a high-resolution transmission electron microscope (HRTEM) might therefore prove useful. Quantitative information can for instance be obtained on the high-energy collective excitations of the valence electrons. The interpretation scheme of the valence loss spectra usually involves a comparison of the experimental data with simulated excitation probabilities. A number of theoretical studies treat the plasmon excitations of single-wall carbon nanotubes.²³⁻³³ Most authors, however, exclusively treat the plasmon dispersion relation.²³⁻²⁸ Plasmon excita-

tion probabilities have only been calculated by Lin *et al.*^{30,31} and Vasvári.³² In their approaches it is assumed that the excitation is induced by a homogeneous electric field. This is true for optical measurements, but does not hold for electrons. In the case of nested concentric-shell fullerenes it has for instance been shown that the plasmon excitation probability depends on the position of the electron probe on the particle.³⁵ This dependence on the impact parameter cannot be reproduced when one assumes that the plasmons are excited by a homogeneous time-dependent electric field. In this contribution we propose a model for the interpretation of EELS data of the plasmons of individual single-wall carbon nanotubes. Our approach basically is an extension of the hydrodynamic formalism of the collective excitations of the valence electrons in carbon nanotubes proposed by Yannouleas *et al.*^{26,28} or Jiang *et al.*²⁴ The extension consists in a high-energy TEM electron that passes through or close by the carbon nanotube. The Coulomb interaction between the two systems has been included and the plasmon excitation probability has been derived for this transmission geometry. The expression of the excitation probability has been evaluated with typical experimental parameters for nanotubes of different radii. Our results can directly be compared to energy filtered TEM images or EEL spectra of individual single-wall carbon nanotubes and therefore should represent a useful basis for the interpretation of such measurements.

II. HYDRODYNAMIC FORMALISM**A. General considerations**

For the simulations of the plasmon-loss spectra of single-wall carbon nanotubes two problems must be solved. First, the electronic properties of a tube have to be modeled. We assume that a single-wall nanotube consists of quasifree electrons confined onto a cylindrical shell of radius a and of infinite length (Fig. 1).³⁴ The electronic properties of the tube

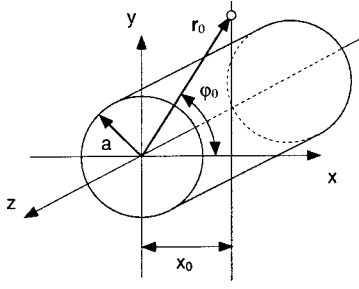


FIG. 1. Geometric parameters of the problem: The probe electron, located at $\mathbf{r}_0(t)$, is traveling parallel to the y axis at a given impact parameter x_0 in negative y direction. Its position is characterized in cylindrical coordinates with the radius $\rho_0(t)$ and the angle $\varphi_0(t)$.

are determined by the dynamics of the electron gas (Sec. II B). Second, the interaction of the TEM probe electrons with the nanotube needs to be taken into account. We suppose independent scattering events, treat the electron classically, and neglect relativistic effects. Furthermore we assume that the electron moves at constant velocity v on a straight line (Fig. 1). These approximations are identical with those made in nonrelativistic local dielectric response theory of the plasmon excitations of nanometer-size particles (for a review, see Ref. 36) and have proven to be valid in various comparative studies between experimental data and simulations. The advantage of this approach is that the potential distribution induced by the TEM probe electron passing through or close by a single-wall carbon nanotube can be calculated explicitly (Sec. II C). The energy loss of the probe electron ΔE can then be deduced from the potential distribution by integration of the elementary work done to the electron by the induced electric field (polarization of the nanotube)

$$\Delta E = \int_{\text{trajectory}} \mathbf{F}(\mathbf{x}, t) \cdot d\mathbf{x} = \int_{\text{trajectory}} (-e) \mathbf{E}(\mathbf{x}, t) \cdot d\mathbf{x}. \quad (1)$$

In the last step of the calculation (Sec. II D) the plasmon excitation probability is deduced from the expression of the energy loss [Eq. (1)] by elimination of ΔE using the relation

$$\Delta E = \int_0^\infty \hbar \omega \frac{dP(\omega)}{d\omega} d\omega. \quad (2)$$

B. Dynamics of the electron gas

We assume that a single-wall carbon nanotube has a cylindrical shell structure whose thickness is negligible in comparison to its diameter. Therefore, the valence electrons are considered to distribute on a cylindrical surface S defined by a delta function in cylindrical coordinates. In consequence the motion of the conduction electrons is also confined in this cylindrical shell. The dynamics of the two-dimensional (2D) electron gas and the effect of the incoming probe electron are treated using the linearized hydrodynamic equations of Bloch [Eqs. (3a)–(3c)].^{36–41}

$$\frac{\partial}{\partial t} \Psi(\mathbf{r}, t) + \gamma \Psi(\mathbf{r}, t) = -\frac{e}{m_e} V(\mathbf{r}, t) + \frac{\beta^2}{n_0} n(\mathbf{r}, t) \Big|_{\mathbf{r} \in S}, \quad (3a)$$

$$\nabla^2 \Psi(\mathbf{r}, t) = \frac{1}{n_0} \frac{\partial}{\partial t} n(\mathbf{r}, t) \Big|_{\mathbf{r} \in S}, \quad (3b)$$

$$\nabla^2 V(\mathbf{r}, t) = \frac{e}{\epsilon_0} \{n(\mathbf{r}, t) + \delta[\mathbf{r} - \mathbf{r}_0(t)]\}. \quad (3c)$$

$\nabla \Psi(\mathbf{r}, t)$ and $n(\mathbf{r}, t)$ are the perturbations of the velocity potential and the charge density of the two-dimensional electron gas, respectively. $V(\mathbf{r}, t)$ represents the electric potential resulting from the electrons on the cylinder and from the probe electron. The constants e , m_e , and n_0 are the elementary charge, the effective electron mass, and the number of electrons participating in the excitation per unit area, respectively. Equation (3a) is the integral form of Newton's equation of motion. Damping needs to be included in order to make the system nonconservative. If this is omitted, the electron does not lose any energy when passing by or through the particle. Damping is contained in the phenomenological friction term, proportional to the velocity potential. The constant of proportionality, the damping coefficient γ , is the inverse of the characteristic collision time. As in the Drude model of metals, γ represents the full width at half maximum of the plasmon resonance peak. The term linear in the electron density can be regarded as diffusion potential of the electrons. β is the root mean square propagation speed of the density disturbance through the electron gas. In the case of a two dimensional electron gas β^2 is related to the Fermi velocity via the relation $\beta^2 = 1/2v_F^2$.⁴² Equation (3b) is the continuity equation for the 2D confined conduction electrons of the cylinder. Since the electrons are confined on a cylindrical surface, Newton's equation of motion [Eq. (3a)] and the continuity equation [Eq. (3b)] must be evaluated on the surface S of the cylinder. Finally, Eq. (3c) is the Poisson equation and has to be solved in all space. $\delta[\mathbf{r} - \mathbf{r}_0(t)]$ represents the probe electron located at position $\mathbf{r}_0(t)$.

C. Solution of the Bloch equations for the nanotube geometry

The solution of the Bloch equations [Eqs. (3a)–(3c)] is straightforward, once the problem is put correctly. In a first step it can be realized that the substitution of Eq. (3b) in the Laplacian of Eq. (3a) allows one to eliminate $\Psi(\mathbf{r}, t)$, so that the original set of equations simplifies to

$$\frac{1}{n_0} \left(\frac{\partial^2}{\partial t^2} + \gamma \frac{\partial}{\partial t} \right) n(\mathbf{r}, t) = -\frac{e}{m_e} \nabla^2 V(\mathbf{r}, t) + \frac{\beta^2}{n_0} \nabla^2 n(\mathbf{r}, t) \Big|_{\mathbf{r} \in S}, \quad (4a)$$

$$\nabla^2 V(\mathbf{r}, t) = \frac{e}{\epsilon_0} \{n(\mathbf{r}, t) + \delta[\mathbf{r} - \mathbf{r}_0(t)]\}. \quad (4b)$$

The appropriate boundary conditions for these equations for the nanotube geometry are (a) the vanishing of the normal component of the velocity perturbation at the surface of the cylinder, (b) the vanishing of the potential as $\rho \rightarrow \infty$, and

(c) the finiteness of the electric potential at the origin. Condition (a) is automatically satisfied, since we assume the electrons to be confined on the cylindrical shell. Conditions (b) and (c) will allow the expansion of the potential and the charge density disturbance in Fourier-Bessel series. The cylindrical shell (nanotube) separates space into two regions, the inside and outside of the nanotube. For the determination of the electric potential it is useful to treat these regions separately. For this purpose, Eq. (4b) is replaced by two equations, which yield the electric potential $V_{\rho>a}(\mathbf{r},t)$ outside and $V_{\rho<a}(\mathbf{r},t)$ inside the tube separately. Both have to satisfy the same differential equation, namely,

$$\left. \begin{aligned} \nabla^2 V_{\rho>a}(\mathbf{r},t) \\ \nabla^2 V_{\rho<a}(\mathbf{r},t) \end{aligned} \right\} = \frac{e}{\epsilon_0} \delta[\mathbf{r}-\mathbf{r}_0(t)]. \quad (5)$$

$V_{\rho>a}(\mathbf{r},t)$ and $V_{\rho<a}(\mathbf{r},t)$ are related to each other by additional boundary conditions which will be discussed below. At this point it has to be realized that the response of the 2D electron gas is frequency dependent. For this reason it is imperative that the equations and the boundary conditions are written in frequency space. Using the convention that the Fourier transform of a function $A(\mathbf{r},t)$ from time into frequency space is given by

$$\tilde{A}(\mathbf{r},\omega) = \int_{-\infty}^{\infty} e^{i\omega t} A(\mathbf{r},t) dt \quad (6a)$$

and the inverse Fourier transform from frequency into time space is given by

$$A(\mathbf{r},t) = \frac{1}{2\pi} \int_{-\infty}^{\infty} e^{-i\omega t} \tilde{A}(\mathbf{r},\omega) d\omega \quad (6b)$$

Equations (4a), (4b), and (5) become

$$-\omega(\omega + i\gamma) \frac{\tilde{n}(\mathbf{r},\omega)}{n_0} = -\frac{e}{m_e} \nabla^2 \tilde{V}(\mathbf{r},\omega) + \beta^2 \nabla^2 \frac{\tilde{n}(\mathbf{r},\omega)}{n_0} \Big|_{\mathbf{r} \in S}, \quad (7a)$$

$$\nabla^2 \tilde{V}_{\rho>a}(\mathbf{r},\omega) = \frac{e}{v\epsilon_0} \delta(x-x_0) \delta(z) e^{i\omega y/v}, \quad (7b)$$

and

$$\nabla^2 \tilde{V}_{\rho<a}(\mathbf{r},\omega) = \frac{e}{v\epsilon_0} \delta(x-x_0) \delta(z) e^{i\omega y/v}, \quad (7c)$$

respectively. Now, the boundary conditions relating $V_{\rho>a}(\mathbf{r},\omega)$ to $V_{\rho<a}(\mathbf{r},\omega)$ in frequency space can be introduced. They are (d) the continuity of the electric potential

$$\tilde{V}_{\rho>a}(\mathbf{r},\omega)|_{\rho \rightarrow a} = \tilde{V}_{\rho<a}(\mathbf{r},\omega)|_{\rho \rightarrow a} \quad (8a)$$

and (e) the relation obtained by integration of the inhomogeneous Maxwell equation relating the displacement field to the charge density

$$\frac{\partial}{\partial \rho} \tilde{V}_{\rho>a}(\mathbf{r},\omega)|_{\rho \rightarrow a} - \frac{\partial}{\partial \rho} \tilde{V}_{\rho<a}(\mathbf{r},\omega)|_{\rho \rightarrow a} = \frac{e}{\epsilon_0} \tilde{n}(\mathbf{r},\omega)|_{\rho \rightarrow a}. \quad (8b)$$

Equations (7a)–(7c) with the boundary conditions Eqs. (8a) and (8b) represent the problem of the plasmon excitations of a single-wall carbon nanotube. The solutions of the inhomogeneous differential equations (7b) and (7c) are composed of a homogeneous and an inhomogeneous term each. Indexing the homogeneous solution *ind* (for induced potential) and the inhomogeneous solution *p* (for particular solution), the solutions of Eqs. (7a) and (7c) read

$$\tilde{V}_{\rho>a}(\mathbf{r},\omega) = \tilde{V}_{\rho>a}^p(\mathbf{r},\omega) + \tilde{V}_{\rho>a}^{\text{ind}}(\mathbf{r},\omega) \quad (9a)$$

and

$$\tilde{V}_{\rho<a}(\mathbf{r},\omega) = \tilde{V}_{\rho<a}^p(\mathbf{r},\omega) + \tilde{V}_{\rho<a}^{\text{ind}}(\mathbf{r},\omega), \quad (9b)$$

respectively. The inhomogeneous term representing the direct potential of the probe electron is the same for both equations. In cylindrical coordinates it is given in terms of a Fourier-Bessel expansion^{43,44}

$$\begin{aligned} \tilde{V}_{\rho<a}^p(\mathbf{r},\omega) &= \tilde{V}_{\rho>a}^p(\mathbf{r},\omega) \\ &= \int_{-\infty}^{\infty} dt e^{i\omega t} \left(\frac{1}{4\pi\epsilon_0} \frac{-e}{|\mathbf{r}-\mathbf{r}_0(t)|} \right) \\ &= \frac{-e}{2\pi\epsilon_0} \sum_{m \geq 0} (2 - \delta_{0,m}) \int_{-\infty}^{\infty} \frac{dq}{2\pi} e^{iqz} \int_{-\infty}^{\infty} dt e^{i\omega t} \\ &\quad \times \cos\{m[\varphi - \varphi_0(t)]\} L_m[|q|\rho, |q|\rho_0(t)], \end{aligned} \quad (10)$$

where

$$\begin{aligned} L_m[|q|\rho, |q|\rho_0(t)] &= K_m(|q|\rho) I_m[|q|\rho_0(t)] \theta[\rho - \rho_0(t)] \\ &\quad + K_m[|q|\rho_0(t)] I_m(|q|\rho) \theta[\rho_0(t) - \rho]. \end{aligned} \quad (11)$$

The function $\theta(x)$ in Eq. (11) is the Heaviside step function given by

$$\theta(x) = \begin{cases} 1 & \text{for } x > 0, \\ 0 & \text{for } x < 0. \end{cases} \quad (12)$$

The homogeneous solutions of Eqs. (7b) and (7c) represent the induced potential due to the charge distribution on the cylindrical shell generated by the probe electron. Yet undetermined, they are expanded into Fourier-Bessel series with coefficients $A_m(q,\omega)$, $B_m(q,\omega)$, $C_m(q,\omega)$, and $D_m(q,\omega)$:

$$\begin{aligned} \tilde{V}_{\rho<a}^{\text{ind}}(\mathbf{r},\omega) &= \frac{-e}{2\pi\epsilon_0} \sum_{m \geq 0} (2 - \delta_{0,m}) \\ &\quad \times \int_{-\infty}^{\infty} \frac{dq}{2\pi} [\cos(m\varphi) A_m(q,\omega) \\ &\quad + \sin(m\varphi) B_m(q,\omega)] e^{iqz} K_m(|q|a) I_m(|q|\rho), \end{aligned} \quad (13a)$$

$$\begin{aligned} \tilde{V}_{\rho>a}^{\text{ind}}(\mathbf{r}, \omega) &= \frac{-e}{2\pi\epsilon_0} \sum_{m \geq 0} (2 - \delta_{0,m}) \\ &\times \int_{-\infty}^{\infty} \frac{dq}{2\pi} [\cos(m\varphi) C_m(q, \omega) \\ &+ \sin(m\varphi) D_m(q, \omega)] e^{iqz} K_m(|q|\rho) I_m(|q|a). \end{aligned} \quad (13b)$$

The unknown series coefficients $A_m(q, \omega)$, $B_m(q, \omega)$, $C_m(q, \omega)$, and $D_m(q, \omega)$ are going to be determined by the boundary conditions Eqs. (8a) and (8b).

In order to find the solution of Eq. (7a) the charge density fluctuation is also written in terms of a Fourier-Bessel series with unknown coefficients $E_m(q, \omega)$ and $F_m(q, \omega)$ which will be determined by substitution in Eq. (7a).

$$\begin{aligned} \tilde{n}(\mathbf{r}, \omega) &= \frac{-e}{2\pi\epsilon_0} \sum_{m \geq 0} (2 - \delta_{0,m}) \delta(\rho - a) \\ &\times \int_{-\infty}^{\infty} \frac{dq}{2\pi} [\cos(m\varphi) E_m(q, \omega) \\ &+ \sin(m\varphi) F_m(q, \omega)] e^{iqz} K_m(|q|a) I_m(|q|a) \end{aligned} \quad (14)$$

The differential Eqs. (7a)–(7c) are now solved. Substitution of $\tilde{V}_{\rho>a}(\mathbf{r}, \omega)$, $\tilde{V}_{\rho<a}(\mathbf{r}, \omega)$, and $\tilde{n}(\mathbf{r}, \omega)$ in the boundary conditions [Eqs. (8a) and (8b)] and in Eq. (7a) yields a set of three linear equations for the six coefficients. Matching the linearly independent sine and cosine terms in each equation, one obtains a set of six equations for six unknowns. The coefficients can thus be determined straightforwardly.

From the continuity of the electric potential [Eq. (8a)] it is immediate that

$$A_m(q, \omega) = C_m(q, \omega) \quad (15a)$$

and

$$B_m(q, \omega) = D_m(q, \omega). \quad (15b)$$

Using the identity^{45,46}

$$I'_m(x)K_m(x) - I_m(x)K'_m(x) = \frac{1}{x}, \quad (16)$$

the boundary condition Eq. (8b) leads to the relations

$$A_m(q, \omega) \frac{1}{a} = -\frac{e}{\epsilon_0} E_m(q, \omega) I_m(|q|a) K_m(|q|a) \quad (17a)$$

and

$$B_m(q, \omega) \frac{1}{a} = -\frac{e}{\epsilon_0} F_m(q, \omega) I_m(|q|a) K_m(|q|a). \quad (17b)$$

The substitution of the expression of the potential [Eqs. (9a) and (9b)] and the charge density fluctuation [Eqs. (14)] into the equation of motion [Eq. (7a)] yields

$$\begin{aligned} &\left[-\omega(\omega + i\gamma) + \beta^2 \left(\frac{m^2}{a^2} + q^2 \right) \right] E_m(q, \omega) \\ &= \frac{en_0}{m_e} \left(\frac{m^2}{a^2} + q^2 \right) [CI_m(q, \omega) + A_m(q, \omega)] \end{aligned} \quad (18a)$$

and

$$\begin{aligned} &\left[-\omega(\omega + i\gamma) + \beta^2 \left(\frac{m^2}{a^2} + q^2 \right) \right] F_m(q, \omega) \\ &= \frac{en_0}{m_e} \left(\frac{m^2}{a^2} + q^2 \right) [SI_m(q, \omega) + B_m(q, \omega)], \end{aligned} \quad (18b)$$

where we have introduced the functions $CI_m(q, \omega)$ and $SI_m(q, \omega)$ defined by

$$\begin{aligned} CI_m(q, \omega) &= 2 \int_{|y|/v}^{\infty} dt \cos(\omega t) \cos[m\varphi_0(t)] \frac{K_m[|q|\rho_0(t)]}{K_m(|q|a)} \\ &+ 2 \int_0^{|y|/v} dt \cos(\omega t) \cos[m\varphi_0(t)] \frac{I_m[|q|\rho_0(t)]}{I_m(|q|a)} \end{aligned} \quad (19a)$$

and

$$\begin{aligned} SI_m(q, \omega) &= 2i \int_{|y|/v}^{\infty} dt \sin(\omega t) \sin[m\varphi_0(t)] \frac{K_m[|q|\rho_0(t)]}{K_m(|q|a)} \\ &+ 2i \int_0^{|y|/v} dt \sin(\omega t) \sin[m\varphi_0(t)] \frac{I_m[|q|\rho_0(t)]}{I_m(|q|a)}. \end{aligned} \quad (19b)$$

Equations (17a)–(18b) form a set of four linear equations for the four remaining coefficients. The solution of the system gives

$$E_m(q, \omega) = \frac{-1}{aK_m(|q|a)I_m(|q|a)} \frac{\epsilon_0}{e} \chi_m(q, \omega) CI_m(q, \omega), \quad (20a)$$

$$F_m(q, \omega) = \frac{-1}{aK_m(|q|a)I_m(|q|a)} \frac{\epsilon_0}{e} \chi_m(q, \omega) SI_m(q, \omega), \quad (20b)$$

$$C_m(q, \omega) = A_m(q, \omega) = \chi_m(q, \omega) CI_m(q, \omega), \quad (20c)$$

and

$$D_m(q, \omega) = B_m(q, \omega) = \chi_m(q, \omega) SI_m(q, \omega), \quad (20d)$$

where $\chi_m(q, \omega)$ is the function

$$\chi_m(q, \omega) = \frac{\Omega_p^2 \left(\frac{m^2}{a^2} + q^2 \right) a K_m(|q|a) I_m(|q|a)}{\omega(\omega + i\gamma) - \beta^2 \left(\frac{m^2}{a^2} + q^2 \right) - \Omega_p^2 a K_m(|q|a) I_m(|q|a) \left(\frac{m^2}{a^2} + q^2 \right)}. \quad (21)$$

Ω_p is given by $\Omega_p = \sqrt{e^2 n_0 / \epsilon_0 m_e}$, where n_0 is the surface electron density of the graphitic shell. Assuming that the layer has a finite thickness d , Ω_p can be related to the bulk electron density of graphite by the relation

$$\Omega_p^2 = \omega_p^2 d, \quad (22)$$

where ω_p is the plasmon resonance frequency of planar graphite, which is related to the bulk charge density N_0 in the usual way:

$$\omega_p = \sqrt{e^2 N_0 / \epsilon_0 m_e}. \quad (23)$$

Note that when the denominator of $\chi_m(q, \omega)$ is put equal to zero, the plasmon dispersion relation is obtained. If the damping coefficient γ and the pressure term β are put equal to zero our result is identical to the particular case of a one-layer tube of the dispersion relation obtained by Yannouleas *et al.*^{26,28}

D. Energy loss of a probe electron

Knowing the electric potential, it is possible now to calculate the energy loss of an electron passing through or close by the single-wall nanotube. For this purpose the Fourier transform of the electric field $\mathbf{E}(\mathbf{x}, \omega) = -\nabla V(\mathbf{x}, \omega)$ is inserted into Eq. (1). Since no volume plasmon can develop on the two-dimensional shell, only the induced potential (surface losses) needs to be considered.

$$\Delta E = \frac{e}{2\pi} \int_{-\infty}^{\infty} dy \int_{-\infty}^{\infty} d\omega e^{-i\omega y/v} \left(\frac{\partial}{\partial y} \tilde{V}^{\text{ind}}(\mathbf{r}, \omega) \right) \Big|_{\mathbf{r}=(x_0, y, 0)}. \quad (24)$$

The induced potential $\tilde{V}^{\text{ind}}(\mathbf{r}, \omega)$ is the homogeneous part of the solution of Eq. (7a).

$$\tilde{V}^{\text{ind}}(\mathbf{r}, \omega) = \begin{cases} \tilde{V}_{\rho < a}^{\text{ind}}(\mathbf{r}, \omega) & \text{for } \rho < a, \\ \tilde{V}_{\rho > a}^{\text{ind}}(\mathbf{r}, \omega) & \text{for } \rho > a. \end{cases} \quad (25)$$

Since the integration needs to be done on a straight line it is useful to reintroduce Cartesian coordinates. $\mathbf{r}_0(t)$, parametrized by $\rho_0(t)$, $\varphi_0(t)$, and z_0 , can be expressed in terms of the parameters of the trajectory of the electron (Fig. 1):

$$\rho_0(t) = \sqrt{x_0^2 + (vt)^2}, \quad (26a)$$

$$\varphi_0(t) = \arccos\left(\frac{x_0}{\rho_0(t)}\right). \quad (26b)$$

Due to symmetry z_0 is assumed to be zero. In the same way the space variable \mathbf{r} with the cylindrical coordinates ρ , φ , and z , can be expressed in terms of the Cartesian coordinates x , y , and z :

$$\rho = \sqrt{x^2 + y^2}, \quad (27a)$$

$$\varphi = \arccos\left(\frac{x}{\rho}\right). \quad (27b)$$

Once the potential substituted in Eq. (24), the excitation probability can be found by elimination of ΔE using Eq. (2). This implies that the ω integral in expression (24) from minus to plus infinity is transformed to an integral from zero to infinity. This is possible since the response of the system is causal. After the necessary transformations the plasmon excitation probability of a single-wall carbon nanotube becomes

$$\begin{aligned} \frac{dP(\omega)}{d\omega} &= \frac{e^2}{\pi^3 \hbar v \epsilon_0} \sum_{m \geq 0} (2 - \delta_{0,m}) \int_0^{q_c} dq \left[\text{Im}[\chi_m(q, \omega)] \right. \\ &\quad \times \left(I_m(qa) \int_{y_0}^{\infty} dy \left\{ \left[\cos(m\varphi) \cos\left(\frac{\omega y}{v}\right) \text{CI}_m(q, \omega) \right. \right. \right. \\ &\quad \left. \left. \left. + \sin(m\varphi) \sin\left(\frac{\omega y}{v}\right) \text{Im}[\text{SI}_m(q, \omega)] \right] K_m(q\rho) \right\} \right. \\ &\quad \left. + K_m(qa) \int_0^{y_0} dy \left\{ \left[\cos(m\varphi) \cos\left(\frac{\omega y}{v}\right) \text{CI}_m(q, \omega) \right. \right. \right. \\ &\quad \left. \left. \left. + \sin(m\varphi) \sin\left(\frac{\omega y}{v}\right) \text{Im}[\text{SI}_m(q, \omega)] \right] I_m(q\rho) \right\} \right) \right]. \end{aligned} \quad (28)$$

If the probe electron passes through the nanotube the integration boundary y_0 is given by $y_0 = \sqrt{a^2 - x_0^2}$ which is half the distance the electron travels inside the tube. If the electron passes outside the tube y_0 is equal to zero. Note that the upper boundary of the integral over q has been put equal to q_c , the critical wave vector.⁴⁷ Above this critical wave vector plasmon excitations can transfer their energy to a single electron and are thus heavily damped (Landau damping).

III. SIMULATED PLASMON EXCITATION PROBABILITIES

A. Technical details

All simulations have been done with the MATHEMATICA software package by Wolfram Research Inc. In order to re-

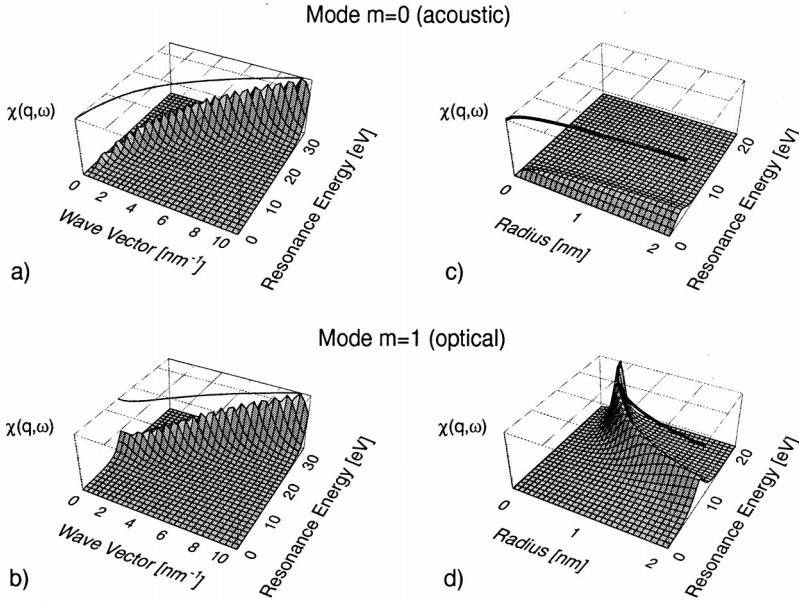


FIG. 2. 3D plot of the imaginary part of the function $\chi_m(q, \omega)$ for the acoustic ($m=0$) and the first optical mode ($m=1$). The maximum of the function indicated by the solid line on the top of each plot determines the resonance frequency. In (a) and (b) the function is plotted for a tube radius of 0.6 nm as a function of the wave vector transfer (dispersion relation). In (c) and (d) $\chi_m(q, \omega)$ is plotted against the nanotube radius for a fixed wave vector transfer of 0.1 nm^{-1} .

duce computation times, we have taken advantage of the possibility to call C or FORTRAN code from within MATHEMATICA.⁴⁸ In particular, all Bessel functions have been evaluated using the FORTRAN NAG library code. Special care has been taken when evaluating the Bessel functions for large or small arguments. A rearrangement of the terms of Eq. (28) allows one to collect I - and K -type Bessel functions in a way that their diverging behavior is compensated (for more details, see Ref. 49).

B. Parameters for the simulations

The excitation probabilities shown in this text have been calculated for TEM probe electrons passing at an impact parameter $x_0=0$ (Fig. 1) for typical experimental conditions. The energy of the incident electrons was assumed to be 100 keV. The diameter of single-wall carbon nanotubes as produced by common methods (arc discharge, laser ablation) is between 1 and 1.5 nm. The simulations have thus been carried out for tubes with 0.5, 0.6, and 0.7 nm radius. Since the mean scattering angle for a probe electron exciting a plasmon is small, we suppose that all scattered electrons are detected by the spectrometer. Experimentally this is realized if no angle limiting apertures are inserted into the column. The maximum scattering angle in this configuration is determined by the plasmon cutoff wave vector. Most simulations have been carried out with a cutoff wave vector of 10 nm^{-1} . This corresponds to a scattering angle of 6 mrad for 100 keV electrons which is of the order of those for the volume plasmon of metals found in the literature.^{47,50} Since the exact value of the cutoff wave vector is not known for single-wall carbon nanotubes simulations have also been carried out for 1 nm^{-1} (0.6 mrad at 100 keV).

The parameters independent of the experimental conditions (intrinsic to nanotube) are the electron density n_0 , the effective electron mass m_e , the damping coefficient γ , and the Fermi velocity v_F (pressure term β). They all appear solely in the expression of the function $\chi_m(q, \omega)$ [Eq. (21)].

It has been shown in Sec. II C that the electron density and the effective mass always appear together and can be collected to form one single parameter Ω_p depending on the resonance energy ω_p of the bulk plasmon and on d , the thickness of the graphitic shell (0.34 nm)

$$\Omega_p^2 = d\omega_p^2 = d \left(\frac{e^2 N_0}{\epsilon_0 m_e} \right). \quad (29)$$

We have restricted the simulations to the excitation of the $\sigma + \pi$ electrons.⁵¹ The simulations have been carried out with two different values for ω_p of the $\sigma + \pi$ electrons: 27.5 and 21.5 eV. The first is the experimentally determined value of the resonance energy of the bulk graphite $\sigma + \pi$ electron plasmon^{52–54} and the second is obtained from estimated values of the electron density and the effective mass.^{26,28} Note that in order to avoid confusion with the plasmon resonance energy of the single-wall tube we call ω_p the resonance parameter. The damping coefficient γ determines the width of the resonance peak. In planar graphite, the full width at half maximum of the $\sigma + \pi$ electron plasmon resonance is 5 eV.⁵⁵ Inspired by this experimental value we have carried out simulations with damping coefficients of 2, 5, and 10 eV. For the Fermi velocity we have taken the value for bulk graphite $v_F = 8.110 \times 10^5 \text{ ms}^{-1}$ given by Wallace.⁵⁶ It turns out that the pressure term is in all circumstances small. In consequence a better estimate of this parameter is not crucial.

C. Dispersion relation

As has been pointed out, the theoretical aspects of the plasmons of single-wall carbon nanotubes have been studied by several authors.^{23–28} It has been established that the spectrum of a single-wall carbon nanotube is composed of a series of contributions which are due to the polar and multipolar oscillation modes characteristic of the cylindrical geometry. Figure 2 shows the imaginary part of the function

$\chi_m(q, \omega)$ for the first two oscillation modes ($m=0$ and $m=1$). For a fixed tube radius ($a=0.6$ nm) the maximum of the function, indicated by the solid line on the top of each plot, as a function of the wave vector q represents the dispersion relation [Figs. 2(a) and 2(b)]. An acoustic dispersion behavior⁵⁷ can be observed for the $m=0$ mode [Fig. 2(a)] while all higher order modes show the characteristics of optical dispersion [Fig. 2(b)]. Figures 2(c) and 2(d) show the dependence of the imaginary part of the function $\chi_m(q, \omega)$ for a fixed wave vector transfer of 0.1 nm^{-1} plotted against the nanotube radius. It can be observed that the resonance energy strongly depends on the nanotube radius. Moreover, this dependence is clearly different for the acoustic [Fig. 2(c)] and for the optical modes [Fig. 2(d)].

With regard to the information accessible by EELS in a HRTEM, Fig. 2 elicits two questions. First, one would like to know which of the modes will give the most important contribution to the spectrum and second, at what energy the plasmon resonance can be observed when all scattering angles are collected. In Sec. III D we discuss the plasmon excitation probabilities for TEM electrons passing through the center of a single-wall nanotube (impact parameter $x_0=0$) calculated with the results of Sec. II. We will show that the simulated data gives the answer to the two questions mentioned above.

D. Excitation probabilities

Figure 3 shows the excitation probabilities obtained with a resonance parameter of 27.5 eV, a damping coefficient of 2 eV and a critical wave vector of 10 nm^{-1} for three different tube radii (0.5, 0.6, and 0.7 nm). The different contributions of the first seven oscillation modes and the total excitation probability (solid line) for each tube radius are shown. The acoustic mode ($m=0$) causes an increase of the excitation probability towards the low energy losses. The first optical ($m=1$) mode determines the onset of the plasmon resonance peak. It can be seen in Fig. 3 that the position of the maximum of the excitation probability depends on the tube radius. The plasmon resonance energy of smaller tubes is higher than that of larger tubes. The modes superior to $m=1$ are responsible for a fine structure in the high-energy flank of the plasmon resonance. The intensity of each contribution decreases as the mode number increases. The energy interval between successive contributions depends on the resonance mode and the tube radius. In larger nanotubes, the oscillation modes are closer together than in smaller ones (Fig. 3). For a given radius the spacing between two successive modes becomes smaller as the mode number is increased.

The cutoff wave vector q_c determines at what rate the intensity of the higher order modes decreases. Figure 4 shows this dependence for a single-wall tube of 0.6 nm radius for two values of q_c (1 and 10 nm^{-1}). The curves have been simulated with a resonance parameter of 27.5 eV and a damping coefficient of 5 eV. It can be observed that for the smaller cutoff wave vectors the first oscillation mode yields the most important contribution and the maximum of the excitation probability is at 14.5 eV. However, for larger val-

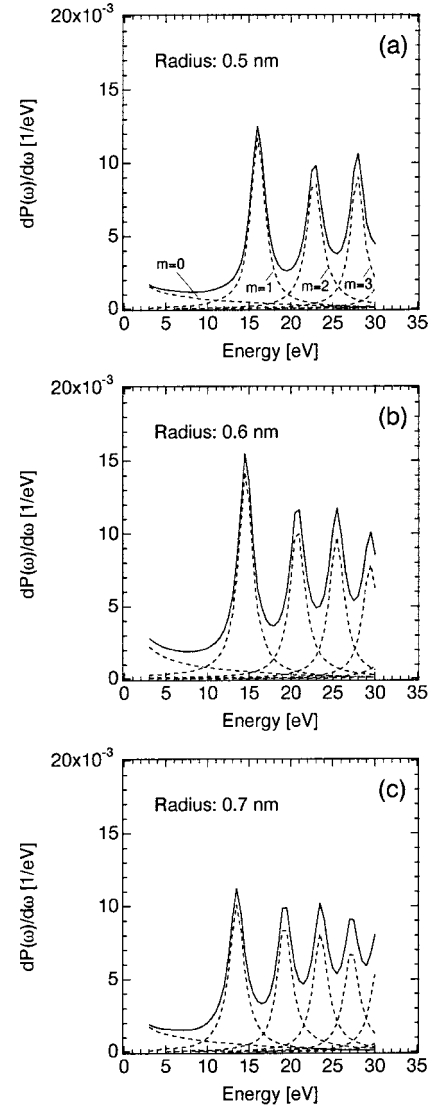


FIG. 3. Plasmon excitation probability for a TEM probe electron passing at an impact parameter $x_0=0$ through single-wall carbon nanotubes of (a) 0.5, (b) 0.6, and (c) 0.7 nm radius. The curves have been simulated for 100 keV electrons assuming a cutoff wave vector of 10 nm^{-1} . The resonance parameter ω_p was 27.5 eV and the damping coefficient γ 2 eV. The total excitation probability is indicated by a solid line. The contributions of the individual modes are dashed.

ues the higher order oscillations become more important as compared to the first order mode. This tendency could become even more pronounced if the restriction of infinitely long nanotubes is omitted. When nanotubes of finite length are considered the wave vector transfer is not only limited by the critical wave vector, but also by the length of the nanotube $1/l \leq q \leq q_c$.³⁶ With regard to the tendency observed in Fig. 4 one can expect the contribution of the higher order modes to be enhanced as compared to the lower order modes. In this case it is possible that the maximum of the plasmon excitation probability is at 20.5 eV, the position of the second order oscillation mode.

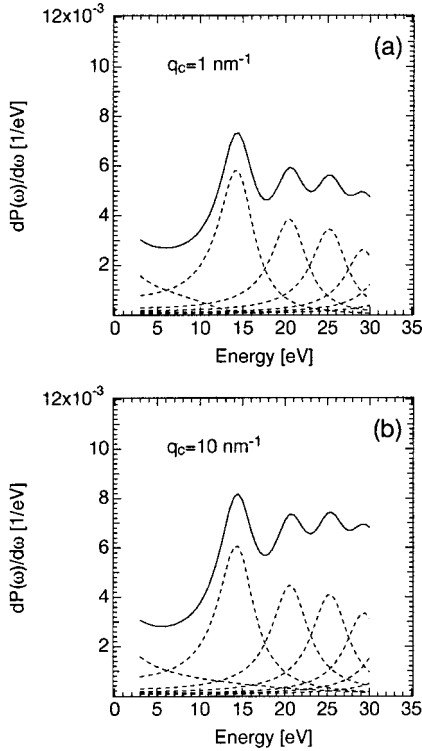


FIG. 4. Plasmon excitation probability for a single-wall carbon nanotube of 0.6 nm radius obtained with a cutoff wave vector of (a) 1 and (b) 10 nm^{-1} . The curves have been simulated for 100 keV electrons with resonance parameter ω_p of 27.5 eV and a damping coefficient γ of 5 eV.

Another situation where the overall maximum of the excitation probability is not at the position of the first order excitation is shown in Fig. 5 where the effect of strong damping is demonstrated (damping coefficient $\gamma = 10$ eV). Hardly any fine structure due to the different modes can be detected and the center of the broad maximum is now found at 23 eV. Figures 2–5 have been simulated with a resonance parameter ω_p of the $\sigma + \pi$ electrons of 27.5 eV as obtained from the experimental EELS data of planar graphite. As discussed in Sec. III B, simulations of the electronic properties of graphite based on the hydrodynamic approach are based

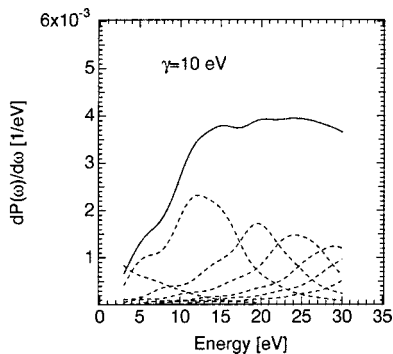


FIG. 5. Plasmon excitation probability for strong damping ($\gamma = 10$ eV) for a single-wall nanotube of 0.6 nm radius. The resonance parameter ω_p was 27.5 eV and the cutoff wave vector q_c was 1 nm^{-1} .

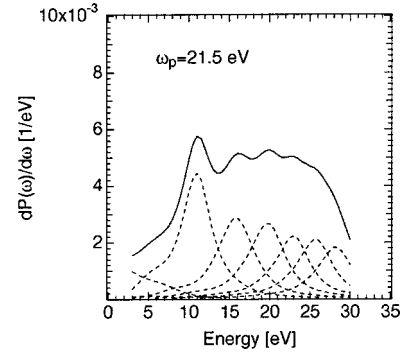


FIG. 6. Excitation probability for a single-wall carbon nanotube of 0.6 nm radius. The simulations have been carried out with a resonance parameter of 21.5 eV, a damping coefficient of 5 eV, and a critical wave vector of 1 nm^{-1} .

on the number of electrons participating in the excitation and their effective mass. Theoretical estimates of these parameters lead to a resonance parameter of 21.5 eV. Figure 6 shows the excitation probability of a single-wall carbon nanotube obtained with 21.5 eV, a damping coefficient of 5 eV, and a critical wave vector of 1 nm^{-1} . It can be seen that taking 21.5 eV instead of 27.5 eV for the resonance parameter causes the plasmon resonance to occur at a much lower energy. In Fig. 6 a small cutoff wave vector and medium damping have been assumed. The maximum of the simulated spectrum is therefore found at the first order excitation mode. Analogous to the case with a resonance parameter of 27.5 eV simulations (not shown) show that strong damping or large cutoff wave vectors cause the maximum to be shifted to the position of the second order resonance.

IV. CONCLUSION

The hydrodynamic theory of a two-dimensional electron gas has been used to derive the probability of a TEM probe electron to lose a given amount of energy when passing through or close by a single-wall carbon nanotube. This plasmon excitation probability is of interest since it can directly be compared to experimental EEL spectra of individual single-wall carbon nanotubes. The simulations indicate that such a spectrum should show a fine structure due to the different oscillation modes possible in the cylindrical geometry. The energy interval between successive maxima in the fine structure decreases when the mode number or the tube radius is increased. In normal experimental conditions the dipolar mode is shown to be the dominant mode which determines the position of the overall maximum of the excitation probability. There are, however, conditions in which the second order mode can dominate the spectrum. This is the case when the plasmon cutoff wave vector is large, when the nanotube is short, or when the plasmon oscillation is strongly damped. The simulations further show that the plasmon oscillation behavior depends on the radius of the nanotube. An increase of the tube radius causes the plasmon resonance to occur at lower energies. It will be interesting to compare the simulations shown here with experimental spectra of individual single-wall carbon nanotubes. Up to now, only mea-

surements on bundles⁵⁸ or electron transparent thin films⁵⁹ have been published. Neither contribution reports any fine structure in the spectra and the plasmon resonance energy is reported to be at 21.5 eV. A comparison with recent experimental data on individual single-wall tubes is presently carried out. The study shows that higher order modes can be observed in the spectra of individual tubes and that there is a rather good agreement between the experimental data and the simulations. The results of this study are subject to another publication.⁶⁰

ACKNOWLEDGMENTS

The authors are grateful to D. Ugarte, L. Forró, and J.-P. Salvetat for many helpful discussions on the subject of EELS and carbon nanoparticles. The experiments have been realized with the help of M. Fazan and the technical staff of the electron microscopy center in Lausanne. Their support is gratefully acknowledged. This work was partially financed by the Swiss National Science Foundation, Grant No. 2100-037660.

*Electronic address: thomas.stoeckli@csem.ch

[†]Present address: Centre Suisse d'Electronique et de Microtechnique (CSEM), Untere Gröndlistrasse 1, CH-6055 Alpnach, Switzerland.

¹S. Iijima and T. Ichihashi, *Nature (London)* **363**, 603 (1993).

²R. Saito, G. Fujita, G. Dresselhaus, and M. S. Dresselhaus, *Appl. Phys. Lett.* **60**, 2204 (1992).

³N. Hamada, S. I. Sawada, and A. Oshiyama, *Phys. Rev. Lett.* **68**, 1579 (1992).

⁴J. W. Mintmire, B. I. Dunlap, and C. T. White, *Phys. Rev. Lett.* **68**, 631 (1992).

⁵A. Thess, R. Lee, P. Nikolaev, H. Dai, P. Petit, J. Robert, Ch. Xu, Y. H. Lee, S. G. Kim, D. T. Colbert, G. Scuseria, T. Tomanek, J. E. Fischer, and R. E. Smalley, *Science* **273**, 483 (1996).

⁶C. Journet, W. K. Maser, P. Bernier, A. Loiseau, M. Lamy de la Chapelle, S. Lefrant, P. Deniard, R. Lee, and J. E. Fischer, *Nature (London)* (London) **388**, 756 (1997).

⁷A. Fonseca, K. Hernadi, P. Piedigrosso, J.-F. Colomer, K. Mukhopadhyay, R. Doome, S. Lazarescu, L. P. Biro, Ph. Lambin, P. A. Thiry, D. Bernaerts, and J. B. Nagy, *Appl. Phys. A: Mater. Sci. Process.* **67**, 11 (1998).

⁸J. H. Hafner, M. J. Bronikowski, B. R. Azamian, P. Nikolaev, A. G. Rinzler, D. T. Colbert, K. A. Smith, and R. E. Smalley, *Chem. Phys. Lett.* **296**, 195 (1998).

⁹K. Tohji, T. Goto, H. Takahashi, Y. Shinoda, N. Shimizu, B. Jeyadevan, I. Matsuoka, Y. Saito, A. Kasuya, T. Ohsuna, K. Hiraga, and Y. Nishina, *Nature (London)* **383**, 679 (1996).

¹⁰S. Bandow, A. M. Rao, K. A. Williams, A. Thess, R. E. Smalley, and P. C. Eklund, *J. Phys. Chem. B* **101**, 8839 (1997).

¹¹G. S. Duesberg, J. Muster, V. Krstic, M. Burghard, and S. Roth, *Appl. Phys. A: Mater. Sci. Process.* **67**, 117 (1998).

¹²E. Dujardin, T. W. Ebbesen, A. Krishnan, and M. M. J. Treacy, *Adv. Mater.* **10**, 611 (1998).

¹³A. G. Rinzler, J. Liu, H. Dai, P. Nikolaev, C. B. Huffman, F. J. Rodríguez-Macías, P. J. Boul, A. H. Lu, D. Heymann, D. T. Colbert, R. S. Lee, J. E. Fischer, A. M. Rao, P. C. Eklund, and R. E. Smalley, *Appl. Phys. A: Mater. Sci. Process.* **67**, 29 (1998).

¹⁴K. B. Shelimov, R. O. Esenaliev, A. G. Rinzler, C. B. Huffman, and R. E. Smalley, *Chem. Phys. Lett.* **282**, 429 (1998).

¹⁵A. Bachtold, M. Henry, C. Terrier, C. Strunk, C. Schöonenberger, J.-P. Salvetat, J.-M. Bonard, and L. Forró, *Appl. Phys. Lett.* **73**, 274 (1998).

¹⁶A. Bezryadin, A. R. M. Verschueren, S. J. Tans, and C. Dekker, *Phys. Rev. Lett.* **80**, 4036 (1998).

¹⁷D. L. Carroll, P. Redlich, P. M. Ajayan, J. C. Charlier, X. Blase, A. De Vita, and R. Car, *Phys. Rev. Lett.* **78**, 2811 (1997).

¹⁸S. Frank, P. Poncharal, Z. L. Wang, and W. A. de Heer, *Science* **280**, 1744 (1998).

¹⁹T. W. Odom, J.-L. Huang, P. Kim, and C. M. Lieber, *Nature (London)* **391**, 62 (1998).

²⁰S. J. Tans, M. H. Devoret, H. Dai, A. Thess, R. E. Smalley, L. J. Geerligs, and C. Dekker, *Nature (London)* **386**, 474 (1997).

²¹J.-P. Salvetat, G. A. D. Briggs, J.-M. Bonard, R. R. Bacsa, A. J. Kulik, T. Stöckli, N. Burnham, and L. Forró, *Phys. Rev. A* **82**, 944 (1999).

²²J.-P. Salvetat, A. J. Kulik, G. A. D. Briggs, J.-M. Bonard, T. Stöckli, N. Burnham, and L. Forró, *Adv. Mater.* **11**, 161 (1999).

²³P. S. Davids, L. Wang, A. Saxena, and A. R. Bishop, *Phys. Rev. B* **49**, 5682 (1994).

²⁴X. Jiang, *Phys. Rev. B* **54**, 13 487 (1996).

²⁵O. Sato, Y. Tanaka, M. Kobayashi, and A. Hasegawa, *Phys. Rev. B* **48**, 1947 (1993).

²⁶C. Yannouleas, E. N. Bogachek, and U. Landman, *Phys. Rev. B* **50**, 7977 (1994).

²⁷P. Longe and S. M. Bose, *Phys. Rev. B* **48**, 18 239 (1993).

²⁸C. Yannouleas, E. N. Bogachek, and U. Landman, *Phys. Rev. B* **53**, 10 225 (1996).

²⁹P. S. Davids, L. Wang, A. Saxena, and A. R. Bishop, *Phys. Rev. B* **51**, 4557 (1995).

³⁰M. F. Lin, K. W.-K. Shung, and K. W. K. Shung, *Phys. Rev. B* **47**, 6617 (1993).

³¹M. F. Lin, D. S. Chuu, C. S. Huang, Y. K. Lin, and K. W.-K. Shung, *Phys. Rev. B* **53**, 15 493 (1996).

³²B. Vasvári, *Phys. Rev. B* **55**, 7993 (1997).

³³M. F. Lin, D. S. Chuu, and K. W.-K. Shung, *Phys. Rev. B* **56**, 1430 (1997).

³⁴In consequence, our model assumes the electronic properties of carbon nanotubes to be quasimetallic.

³⁵T. Stöckli, J.-M. Bonard, A. Chätelain, Z. L. Wang, and P. Stadelmann, *Phys. Rev. B* **61**, 5751 (2000).

³⁶Z. L. Wang, *Micron* **27**, 265 (1996).

³⁷F. Bloch, *Z. Phys.* **81**, 363 (1933).

³⁸H. Jensen, *Z. Phys.* **106**, 620 (1937).

³⁹J. Crowell and R. H. Ritchie, *Phys. Rev.* **172**, 436 (1968).

⁴⁰R. Ruppin, *J. Phys. Chem. Solids* **39**, 233 (1978).

⁴¹F. Fujimoto and K. Komaki, *J. Phys. Soc. Jpn.* **25**, 1678 (1968).

⁴²A. L. Fetter, *Ann. Phys. (N.Y.)* **88**, 1 (1974).

⁴³Y. T. Chu, R. J. Warmack, R. H. Ritchie, J. W. Little, R. S. Becker, and T. L. Ferrell, *Part. Accel.* **16**, 13 (1984).

⁴⁴J. D. Jackson, *Classical Electrodynamics* (John Wiley and Sons, New York, 1975).

⁴⁵M. Abramowitz and I. A. Stegun, *Handbook of Mathematical Functions* (Dover Publications, New York, 1965).

- ⁴⁶G. N. Watson, *A Treatise on the Theory of Bessel Functions* (Cambridge University Press, Cambridge, 1996).
- ⁴⁷R. F. Egerton, *Electron Energy-Loss Spectroscopy in the Electron Microscope* (Plenum Press, New York, 1996).
- ⁴⁸S. Wolfram, *The Mathematica Book* (Addison-Wesley, New York 1996).
- ⁴⁹T. Stöckli, Ph.D. thesis, Swiss Federal Institute of Technology of Lausanne, 1999.
- ⁵⁰H. Raether, *Excitation of Plasmons and Interband Transitions by Electrons* (Springer, Berlin, 1980).
- ⁵¹Our model could also be used to simulate the excitation of the π electrons, simply by choosing the appropriate parameters. Treating the $\sigma + \pi$ and the π electrons separately is equivalent to the two-fluid hydrodynamic approach proposed by Jiang (Ref. 24) for the calculation of the plasmon dispersion relation of a single-wall carbon nanotube.
- ⁵²E. D. Palik, *Handbook of Optical Constants of Solids* (Academic Press, New York, 1985).
- ⁵³E. A. Taft and H. R. Philipp, Phys. Rev. **138**, 197 (1965).
- ⁵⁴H. Venghaus, Phys. Status Solidi B **71**, 609 (1975).
- ⁵⁵J. Daniels, C. Festenberg, H. Raether, and K. Zeppenfeld, *Optical Constants of Solids by Electron Spectroscopy* (Springer, Berlin, 1979).
- ⁵⁶P. R. Wallace, Phys. Rev. **71**, 622 (1947).
- ⁵⁷N. W. Ashcroft and N. D. Mermin, *Solid State Physics* (Saunders College, Fort Worth, 1976).
- ⁵⁸T. Kuzuo, M. Terauchi, M. Tanaka, and Y. Saito, Jpn. J. Appl. Phys. Part 2 **33**, L1316 (1994).
- ⁵⁹T. Pichler, M. Knupfer, M. S. Golden, J. Fink, A. Rinzler, and R. E. Smalley, Phys. Rev. Lett. **80**, 4729 (1998).
- ⁶⁰T. Stöckli, J.-M. Bonard, A. Châtelain, Z. L. Wang, and P. Stadelmann (unpublished).